Energy-level localization in Bragg-confined asymmetric coupled quantum wells studied by electric field modulation spectroscopy

M. Levy and R. Beserman
Solid State Institute and Physics Department, Technion, Israel Institute of Technology, Haifa 32000, Israel

R. Kapon and A. Sa'ar
Department of Applied Physics, The Fredi and Nadine Hermann School of Applied Science, The Hebrew University of Jerusalem, Jerusalem 91904, Israel

V. Thierry-Mieg and R. Planel
Laboratoire de Microstructures et Microelectronique—CNRS, 196 Avenue H. Ravera, BP107, 92225 Bagneux, France
(Received 30 May 2000; published 30 January 2001)

Electronic Bragg mirrors are used to confine carriers at energy levels above the barrier height in asymmetric coupled quantum wells. An electric field inside the quantum structure is created by transferring carriers from a wide quantum well into a narrow one. Two classes of above-the-barrier states are resolved by using modulated resonant Raman spectroscopy. The first level is the resonant one, which is highly localized by the Bragg reflector above the asymmetric quantum well and is redshifted when a photogenerated local electric field is created in the asymmetric quantum well region. The second class of levels, which extend mainly above the reflectors region, is seen by photoluminescence and photoluminescence excitation measurements. It is less shifted than the resonant level, when the photogenerated local field is applied, which is due to the smaller localization of these states in the asymmetric coupled quantum wells. We used modulated photoluminescence and Raman spectroscopy to resolve the Stark shifts of the bound and continuum levels as a function of the infrared photoexcitation intensity. Our results indicate that because of the photoinduced electric field, the shifts of the above the barrier levels are linked to their degree of localization. These shifts are much stronger than those of the bound states inside the well and a model is proposed to explain the shifts of the continuum and bound levels using perturbation theory.

DOI: 10.1103/PhysRevB.63.075312 PACS number(s): 73.61.Ey, 78.20.−e, 78.55.−m, 78.55.Cr

I. INTRODUCTION

Localization of carriers in energy levels above the barrier height of a quantum well (QW) has attracted considerable attention in recent years due to fundamental interest and potential applications such as infrared detectors. In a QW, we distinguish between bound states below the energy gap of the barrier and the states whose energies are above the barrier by their degree of localization. While the bound states are highly localized in the QW region, the continuum energy levels generally extend above the barriers and the QW's regions. The continuum states that are more localized are often referred to as quasibound states. These quasibound states have an enhanced probability to be found in the QW region. This enhancement takes place when the QW width fulfills the transmission resonance condition:

$$L_{\mathrm{QW}}=(n\times\lambda_{\mathrm{QW}})/2, \tag{1.1}$$

where L_{QW} is the width of the QW, λ_{QW} denotes the carrier De-Broglie wavelength in the QW, and n is an integer. These quasibound states were studied by Resonant Raman Scattering (RRS) by Zucker *et al.*[1]

These quasibound states are localized in the QW region for a finite time and finally escape to the barrier region. By replacing the barriers on each side of the QW with Bragg reflectors,[2] a further enhancement in the localization of these quasibound states is obtained by strongly reducing the penetration of the envelope wave function into the reflectors regions. These Bragg reflectors are finite superlattice (SL) composed of a series of QW's and barriers that are designed so that the envelope wave function of the quasibound states will interfere destructively in the reflectors region and obey the Fabry-Perot condition,

$$L_{w,b}=(n\times\lambda_{w,b})/4, \tag{1.2}$$

where $L_{w,b}$ are the width of the QW and barrier, respectively, in the SL section (reflector region), $\lambda_{w,b}$ denotes the electron De-Broglie wavelength in the QW and barrier, respectively, and n is an integer.

These two conditions (1.1) and (1.2) are the criteria that give highly localized states in the QW region. These states with energy above the barrier are often referred to as Braag states.[3–8]

The addition of reflectors modifies the total energy spectrum. In the SL region new levels appear in the wells at energy below the energy of the barrier.

On the other hand, the situation at energies above the barrier becomes much more complex. In the absence of a QW, when only the SL is present at energies above the barrier, we have a set of minibands and minigaps. When a QW is introduced, classes of states appear in the gaps created by the SL structure. These states common to the QW and to the SL structures have different degrees of localization in the QW area, which demands a redefinition and a new investi-

gation of the states with energies higher than the barrier energy. Here we investigate a device that contains electronic Bragg mirrors instead of wide barriers. These Bragg mirrors allow the formation of states that are confined above the QW and of states spread above the barrier. In addition, this structure also incorporates the ability to study the confinement of these states by a modulation technique that is based on the creation of a local dc electric field by charge transfer in a coupled quantum wells region. The incorporation of these two unique features makes it possible to study the physics of the above the barrier states by investigating their localization and their behavior under applied photoexcited electric fields. The transfer of charges by IR excitation from a wide QW (WQW) into a narrow QW (NQW) was originally designed as an IR detector, the Bragg reflectors were added to increase the localization of the wave functions.

In this paper we study the localization of the different classes of states inside the QW and above the barrier by using the recently developed method of locally modulated resonant Raman scattering[9] and modulated photoluminescence. The basic idea of these techniques is to generate a local dc electric field, inside the QW, by intersubband transitions (ISBT). This local field enables the modulation of energy states according to their degree of localization.

The local electric field in the structure was obtained by using asymmetric coupled QW's (ACQW) to transfer carriers from a WQW into a NQW through an intermediate barrier [Fig. 1(a)]. This charge transfer was created by the 10.6 μm line of a CO_2 laser, which induced intersubband electronic transition from the ground state of the WQW into the ground state of the NQW via an electronic state common to the ACQW. In Fig. 1(a), we schematically show the ISBT process. These electronic transitions give rise to a local electric field across the ACQW region but not outside the ACQW in the Bragg reflectors region.

Under resonant conditions, when the CO_2 pumping laser energy is equal to the energy difference between the ground state of the WQW and the first electronic level of the ACQW E_3, i.e., when charge transfer takes place, local modulation of the photoluminescence (MPL) signal inside the QW states, as well as local modulation of the resonant Raman scattering signal (MRRS) from the above the barrier localized states are observed.

By using MPL and MRRS, we measured the energy shift of the Bragg state, while less localized states showed smaller shifts. The size of the shift of these states is linked to their degree of localization in the ACQW region and we explain these shifts quantitatively using perturbation theory. Therefore, we were able to distinguish between the different states by their amount of localization and define several classes of states.

The paper is organized as follows: In Sec. II we describe the sample and experiment, Sec. III presents the experimental results which are discussed in Sec. IV. We conclude in Sec. V.

II. EXPERIMENT

The sample was grown by molecular beam epitaxy on a semi-insulating substrate. It consists of 25 periods of a Bragg

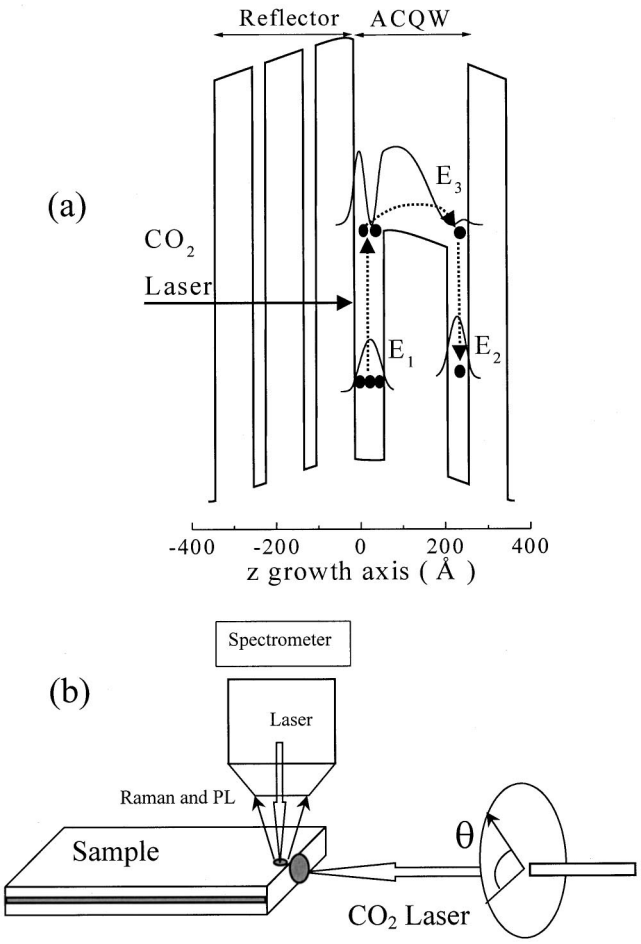

FIG. 1. (a) Schematic description of the conduction band showing the Bragg reflector and the ACQW. Also shown is the intersubband excitation process and the charge carrier transfer from the WQW to the NQW that generates the static electric field. (b) Schematic description of the experimental setup of the MPL and MRRS.

confining structures. The Bragg confining structure is composed of an ACQW that is grown between two $GaAs/Al_{0.34}Ga_{0.66}As$ Bragg mirrors. The ACQW is composed of a 7 nm-GaAs WQW, a 15 nm-$Al_{0.2}Ga_{0.8}As$ intermediate barrier and a 5 nm-GaAs NQW. Each Bragg mirror consists of four periods of 3 nm-GaAs QW and 9 nm-$Al_{0.34}Ga_{0.66}As$ barrier. The structure was designed so that the lowest ground states E_1 and E_2 are located in the WQW and NQW, respectively, and the third level E_3 extends over the entire ACQW and it's energy is 115 meV higher than E_1 [see Fig. 1(a)]. In order to populate the ground electronic state E_1, the sample was modulation doped with an electron concentration of $2\times10^{11}\,cm^{-2}$. The Si dopant was deposited in a GaAs QW of the SL section that forms the Bragg reflector, creating a two-dimensional electron gas in the WQW region (Fig. 1). The whole structure was capped with a 15 nm-GaAs layer.

The sample was cleaved into a stripe geometry and was glued to a cold finger of an Oxford microstat and held at 10 K. The CO_2 laser was focused into a spot of $\cong$100 μm on the cleaved facet using a Ge lens[9] [see Fig. 1(b)]. The intensity

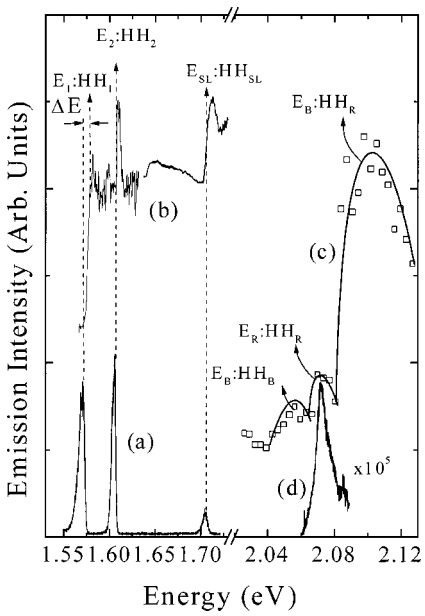

FIG. 2. PL and PLE of bound and above the barrier energy levels in the Bragg-confined structure. (a) PL of the three lowest bound subbands. (b) PLE of the bound levels monitored at the WQW energy transition. (c) PLE of above the barrier energy states monitored at the WQW energy transition. (d) PL of above the barrier states in the reflector region.

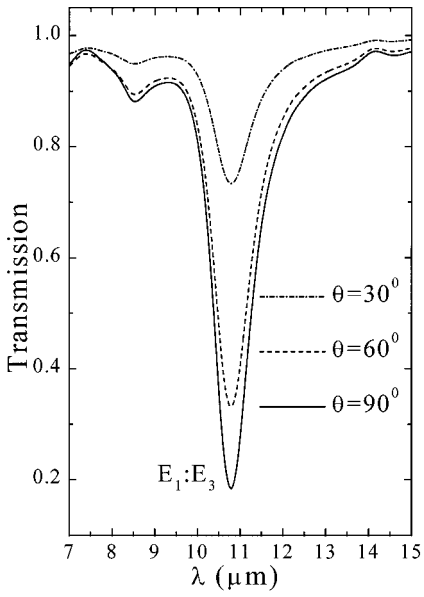

FIG. 3. IR absorption polarization spectroscopy. θ is the angle between the IR electric field vector and the layers plane.

of the CO_2 laser varied from 1 to 10 kW/cm^2. All photoluminescence (PL) and Raman spectra were recorded in the back-scattering geometry, and were excited by a cw dye laser pumped by an Ar^+ laser in the 1.96–2.16 eV range. Low excitation power of up to 1.5 mW focused on a 3 μm diameter point was used for all PL and RRS measurements. The scattered radiation was analyzed by a triple monochromator DILOR micro-Raman spectrometer, and the signal was detected by a CCD camera.

III. RESULTS

A. PL and PLE spectroscopy

Figure 2 shows the PL and the photoluminescence excitation (PLE) spectra from the bound states inside the well and from the continuum states. The PL spectrum [Fig. 2(a)] shows three peaks $E_1{:}HH_1$, $E_2{:}HH_2$, and $E_{\rm SL}{:}HH_{\rm SL}$ at 1.57 eV, 1.605 eV, and 1.705 eV, respectively, which are identified as a recombination of electrons and holes from bound states in the WQW, NQW, and from the bound level in the QW of the Bragg reflectors, respectively. Figure 2(b) shows the PLE spectrum of bound states monitored at the WQW transition energy. We identify the three transitions indicated above. We also observe a Stokes shift of $\Delta E = 8$ meV of the $E_1{:}HH_1$ (WQW) transition between the PL [Fig. 2(a)] and the PLE [Fig. 2(b)] signals. The two-dimensional concentration in the WQW was estimated from this energy shift to be[10] $n = 2\times10^{11}\,{\rm cm}^{-2}$.

The PLE spectrum from energy states above the barrier monitored at the WQW energy ($E_1{:}HH_1$) is shown in Fig. 2(c) (The barrier energy of $Al_{0.34}As_{0.66}As$ at 10 K is 2 eV.) Three continuum transitions are resolved at 2.052 eV, 2.07 eV, and 2.082 eV, which are identified as the Bragg transition $E_B{:}HH_B$ (B stands for Bragg), the reflector transition $E_R{:}HH_R$ (R stands for reflector) and the $E_B{:}HH_R$ transition. We assign the $E_B{:}HH_B$ transition and $E_B{:}HH_R$ to a class of highly localized energy states in the ACQW, while $E_R{:}HH_R$ is mostly localized in the reflector region.

The high-energy part of the PL [Fig. 2(d)] near 2.07 eV, is assigned to the transition $E_R{:}HH_R$ and it is seen also in the PLE spectrum. The PL signal from this state is an indication of the localization of this level in the reflector region. The electronic transitions $E_B{:}HH_B$ and, to a lesser extent, the transition $E_B{:}HH_R$ are more localized in the ACQW region than the $E_R{:}HH_R$ one. As a result, carriers in the Bragg-confined energy levels E_B and HH_B decay more rapidly to lower subbands and, therefore, do not recombine radiatively at this energy. On the other hand, carriers with wave functions that are more localized in the reflector region have a longer lifetime[6] due to smaller overlap with the lower subbands and contribute significantly to the PL signal.

B. Effect of photoexcitation

1. Levels bound inside the wells

Figure 3 shows the IR absorption spectrum. The absorption peak is near 10.6 μm (117 meV) and it is identified as the $E_1 \rightarrow E_3$ energy transition in good agreement with our calculated energy difference of 115 meV. Furthermore, Fig. 3 shows that this peak obeys the ISBT selection rules,[11] θ is the angle between the electric field of IR radiation and the layers plane [Fig. 1(b)]. Therefore, when irradiating the sample with a 10.6 μm line of a CO_2, carriers that are located in the ground state (E_1) in the WQW, are resonantly excited by a CO_2 laser to E_3, which is common to the entire ACQW. Some of these carriers lose their energy by phonon-assisted relaxation processes and decay to the state E_2 and

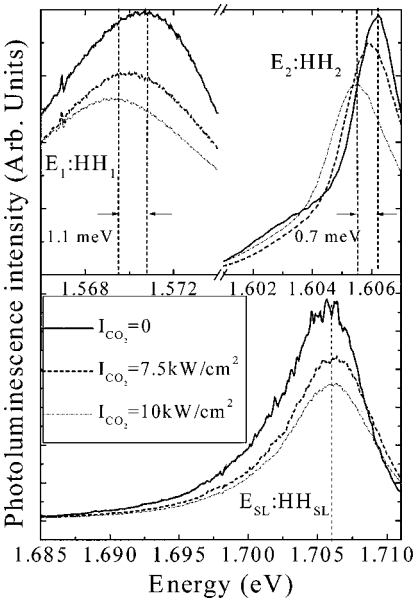

FIG. 4. PL spectra of the bound states under various infrared excitation intensities.

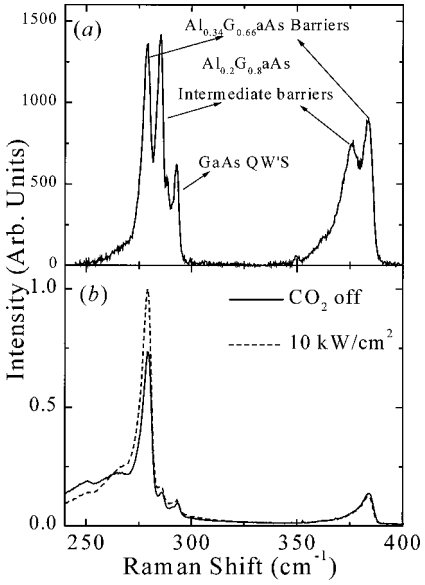

FIG. 5. (a) Raman spectrum of the Bragg-confined structure. (b) Raman spectrum taken without and with a 10 kW/cm^2 CO_2 laser, with the probing dye laser set at 2.1 eV.

stay there because the tunneling to E_1 is very inefficient, inducing a local dc electric field across the ACQW.[12]

In order to investigate the effect of electric field on the energy levels inside the wells, we measured the redshifts of the PL signals $E_1{:}HH_1$, $E_2{:}HH_2$, and $E_{\mathrm{SL}}{:}HH_{\mathrm{SL}}$ as a function of the CO_2 excitation intensities. Figure 4 shows the PL spectra of these bound levels for three values of CO_2 excitation intensity, the maximum value is 10 kW/cm^2. The results indicate that at the highest excitation power (10 kW/cm^2) the level $E_1{:}HH_1$, which is a bound state inside the WQW, redshifts by 1.1 meV, the level $E_2{:}HH_2$, which is a bound state inside the NQW shifts by 0.7 meV, and the level $E_{\mathrm{SL}}{:}HH_{\mathrm{SL}}$, which is a bound state inside the SL does not shift at all, as expected, because it lies outside the ACQW where the influence of the electric field is felt. These results indicate that the shifts depend on the QW size.

Under these IR excitation intensities, we were unable to measure the anti-Stokes-Raman component. We also checked that there was no shift in the frequency of the phonons under these excitation, therefore, we estimate the sample temperature under CO_2 laser illumination to be lower than 40 K. If the redshift was due to heating it would have induced a redshift of the $E_{\mathrm{SL}}{:}HH_{\mathrm{SL}}$ transition that is not seen. The observed redshifts are not caused by heating.

2. Levels in the continuum

Among the three electronic transition from levels in the continuum, $E_B{:}HH_B$, $E_R{:}HH_R$, and $E_B{:}HH_R$, only the level $E_R{:}HH_R$ could be resolved by PL measurements, the other continuum transitions $E_B{:}HH_B$ and $E_B{:}HH_R$ were resolved either by PLE or RRS. Therefore, in order to investigate the degree of localization of these three levels we studied the influence of the photoinduced electric field by PL and RRS. We measured the shift induced by the photogenerated electric field on the different levels illuminated by various IR excitation intensities.

In the structure, we have three different layers GaAs, $Al_{0.2}As_{0.8}As$, and $Al_{0.34}Ga_{0.66}As$ that constitute a single unit cell. Therefore, the Raman spectrum is composed of the following phonon frequencies [Fig. 5(a)]: 292 cm^{-1} (36.2 meV) from the GaAs layers, 285 cm^{-1} (35.3 meV) and 376 cm^{-1} (46.6 meV) from the $Al_{0.2}As_{0.8}As$ layer, which are the GaAs-like and AlAs-like modes, respectively. The peaks at 280 cm^{-1} (34.7 meV) and 382 cm^{-1} (47.3 meV) are the GaAs-like and AlAs-like modes of the $Al_{0.34}As_{0.66}As$ layer, respectively. Figure 5(b) shows the effect of the CO_2 laser on the Raman spectrum (with the probing dye laser energy set at 2.1 eV). At this laser energy, the phonon modes of the GaAs and $Al_{0.2}As_{0.8}As$ layers are very weak. The effect of the CO_2 laser on the Raman spectrum is to enhance the GaAs-like mode intensity while the AlAs-like mode intensity is unchanged. By measuring the intensity of these peaks as a function of the dye laser energy, we get three RRS profiles, one for the GaAs, one for $Al_{0.2}As_{0.8}As$, and one for $Al_{0.34}As_{0.66}As$ (these spectra are shown in Fig. 6). In the laser energy range 2.02–2.1 eV, we have the normal RRS process, when the laser energy equals that of an electronic transition at 2.052 eV, 2.07 eV, or 2.082 eV, the Raman intensity is enhanced. In the energy range 2.1–2.15 eV, the outgoing resonance enhances the Raman intensity at energies equal to that of the electronic transition plus the phonon energy. We resolve in these spectra, three electron-hole transitions at 2.052, 2.070, and 2.082 eV that are identified as $E_B{:}HH_B$, $E_R{:}HH_R$, and $E_B{:}HH_R$, respectively, and are in good agreement with the energies measured by PL and PLE. The level $E_B{:}HH_B$ at 2.052 eV is seen mainly in the RRS spectra of the GaAs [black squares in Fig. 6(a)] and in the $Al_{0.2}As_{0.8}As$ layers [Fig. 6(b)]. This level redshifts by 14 ± 2 meV under an infrared excitation intensity of 8 kW/cm^2.

The higher energy transitions $E_R{:}HH_R$ near 2.07 eV and $E_B{:}HH_R$ at 2.082 eV were seen in the MRRS spectra of all

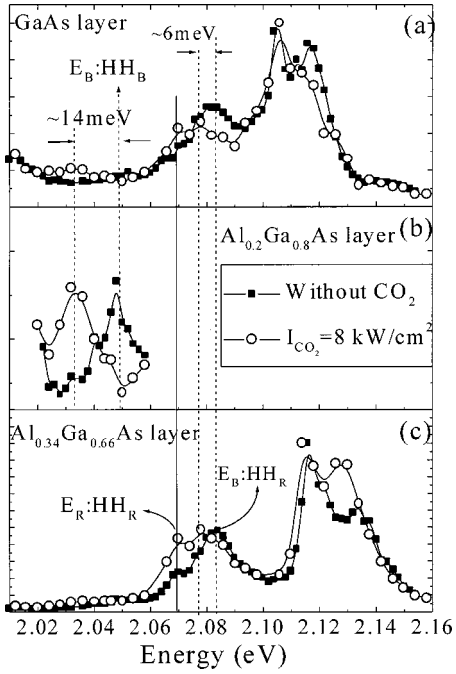

FIG. 6. RRS of the above barrier levels without (solid squares) and with (open circles) IR excitation of 8 kW/cm^2. (a) RRS from the GaAs layers (b) is the AlAs-like RRS profiles, respectively, from the $Al_{0.2}Ga_{0.8}As$ layers (c) AlAs-like RRS profile from the $Al_{0.34}Ga_{0.66}As$ layers.

layers, but were better defined in the GaAs and $Al_{0.34}As_{0.66}As$ layers [Figs. 6(a) and 6(c)]. Under an infrared excitation intensity of 8 kW/cm^2, the level $E_R{:}HH_R$ shifts by less than 2 meV, which is our energy resolution. The results of the MRRS experiment for the level $E_B{:}HH_R$ (2.082 eV) are shown in Figs. 6(a) and 6(c) and indicate a redshift of 6 ± 2 meV under the same infrared excitation (8 kW/cm^2).

The two peaks near 2.11 eV are the outgoing Raman signal of the two transitions E_R: HH_R and E_B HH_R which are found at one phonon energy away from the incoming Raman signals.[1] The out going signals are shifted exactly as the incoming signals under infrared excitation. In order to resolve the exact shift of the level $E_R{:}HH_R$, we used the PL signal of this transition. We measured the PL signal of this transition under various infrared illumination intensities. Figure 7 shows that this level is gradually redshifted with increasing infrared excitations. The maximum redshift is 2.2 meV under the highest infrared excitation intensity of 10 kW/cm^2 and the full width at half maximum (FWHM) $=14.8$ meV is independent of the CO_2 laser power within our experimental error (0.3 meV).

IV. DISCUSSION

A. Calculation of the energy spectrum of the sample

The conditions 1.1 and 1.2 were taken into account when we designed the structure, but the actual electronic structure simulation is based on a numerical solution of the Ben-Daniel-Duke and the Poisson equations for the valence and conduction bands[13,14] using periodic boundary conditions.

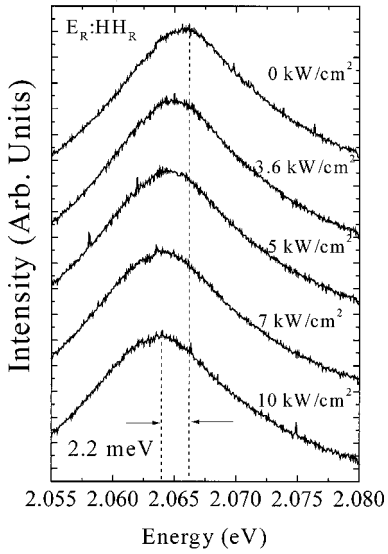

FIG. 7. PL spectrum of the continuum level $E_R{:}HH_R$ under several infrared excitation.

Figure 8 shows schematically the result of the numerical solution. The following features are observed: First, we see electrons (E_1 and E_2) and holes (HH_1 and HH_2) that are highly localized in the ACQW region. Second, we have bound electrons (E_{SL}) and holes (HH_{SL}) in the reflector region, which are highly localized in the SL's that constitute the Bragg reflectors. Normally, the SL states are degenerate and would constitute a miniband, but because of the modulation doping built-in electric field, this degeneracy is lifted

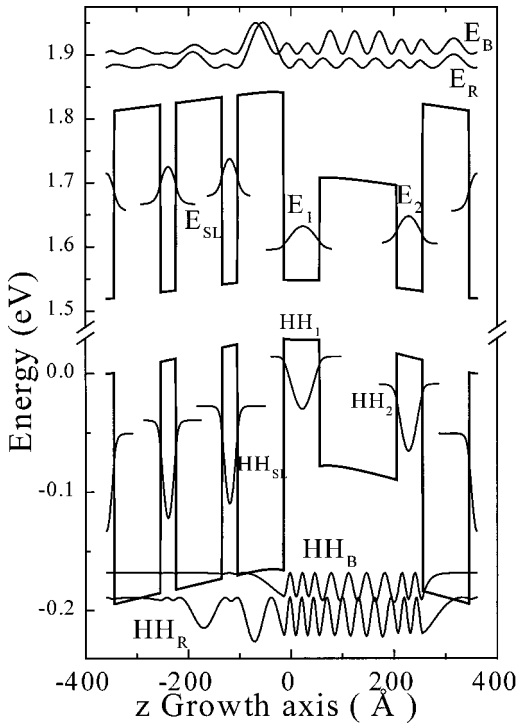

FIG. 8. Conduction and valence energy states of the Bragg-confined structure, calculated by solving self-consistently the Ben Daniel-Duke and the Poisson equations.

TABLE I. Experimental and calculated energy transitions for bound and continuum states.

	$E_1:HH_1$ (eV)	$E_2:HH_2$ (eV)	$E_{SL}:HH_{SL}$ (eV)	$E_B:HH_B$ (eV)	$E_R:HH_R$ (eV)	$E_B:HH_R$ (eV)
Calculation	1.571	1.606	1.706	2.058	2.072	2.085
Experiment	1.57	1.605	1.705	2.052	2.07	2.082

and these states do not interact. The calculated transition energies of the three bound states $E_1:HH_1$, $E_2:HH_2$, and $E_{SL}:HH_{SL}$ are in good agreement with our experimental results (Table I).

Figure 8 also shows the energy levels above the barrier. Two electronic states E_B and E_R, as well as two hole states HH_B and HH_R, are shown. In principle, these states can give rise to four transitions, namely: $E_B:HH_B$, $E_R:HH_R$, $E_B:HH_R$, and $E_R:HH_B$. However, due to very small overlap integral, the last transition $E_R:HH_B$ is not seen. The calculated transition energies of the three transitions $E_B:HH_B$, $E_R:HH_R$, and $E_B:HH_R$ are given in Table I and are also in agreement with our experimental results. In order to compare the localization of the different states, we calculated ρ, the probability to find the carriers in the ACQW

$$\rho^n_{i=e,h}=\int_{\mathrm{ACQW}}|\psi^n_i(z)|^2dz, \tag{4.1}$$

where the integration is along the growth direction, and $\psi^n_i(z)$ is the envelope wave function of the nth state, and i is either an electron or a hole. The values of ρ for the different energy states are summarized in Table II. From these values we deduce that the most localized state in the ACQW region are the Bragg states (E_B and HH_B). On the other hand, the reflector states (E_R and HH_R) are the ones that are the less localized in the ACQW region, while the states E_B and HH_R are in between.

B. The local-field effect

In order to quantitatively explain the shifts of the energy levels under the induced dc local electric field, we propose to adapt to our asymmetric structure the perturbative description, which explains the Stark effect in a symmetric QW.[11] The total Hamiltonian can be written

$$H=H_0+H_1$$

$$H_1=\begin{cases} q\times F_{\mathrm{local}}\times z & z\in \mathrm{ACQW} \\ 0 & \text{elsewhere.}\end{cases} \tag{4.2}$$

TABLE II. The probability of finding carriers in the ACQW ρ [Eq. (4.1)] calculated for the heavy holes (HH) and electrons (E) of the three above the barrier transitions.

	E_B	HH_B	E_R	HH_R	E_B–HH_R
ρ (in % of the total probability)	0.52	0.87	0.13	0.54	0.52–0.54

H_0 denotes the unperturbed Ben-Duke Hamiltonian for the conduction and valence bands. H_1 is the perturbation Hamiltonian, q is the carrier charge, F_{local} is the photogenerated dc local electric field, and z is the carrier position along the growth direction with respect to the center of the QW. Using the standard procedure of the perturbation theory, the energy correction ΔE retaining the second-order term is given by

$$\begin{aligned}\Delta E^n&=\langle H_1\rangle\\&=|e|(\langle z\rangle^{n,n}_h-\langle z\rangle^{n,n}_e)F_{\mathrm{local}}\\&\quad-e^2{F_{\mathrm{local}}}^2\sum_{i=h,e}\sum_{n\neq m}\frac{|\langle z\rangle^{n,m}_i|^2}{E_m-E_n}\\&\quad\times\langle z\rangle^{n,m}_i=\int_{\mathrm{ACQW}}(\psi^*_1)^n z\,\psi^m_1dz,\end{aligned} \tag{4.3}$$

where $\langle z\rangle$ is the carrier average position with respect to the center of the QW and $\psi^n_{i=h,e}$ is the unperturbed n state heavy hole or electron envelope wave function, respectively. The summation in the second-order term is over heavy hole and electron states and it includes virtual transition $n\rightarrow m$. However, only the first nearest energy states contribute significantly to this term, therefore, only contributions from the closest energy levels were taken into account.

Contrary to the symmetric QW, in the ACQW the carriers wave functions in the WQW and NQW tend to leak more into the intermediate barrier and, therefore, have an asymmetrical shape as shown in Fig. 8. Hence, the first-order term does not vanish. Obviously, the first-order term is stronger than the second-order term, and as the field increases, the dipole $|e|(\langle z\rangle^{n,n}_h-\langle z\rangle^{n,n}_e)$ in the first-order correction increases, electrons and holes tend to accumulate at opposite edges of the well, and the limit of $(\langle z\rangle^{n,n}_h-\langle z\rangle^{n,n}_e)$ tends to equal the QW well width l. Therefore, we expect the ground-state transition $E_1:HH_1$ in the WQW to show a larger shift than the NQW ground-state $E_2:HH_2$ transition when the photoinduced electric field is applied. As for the states above the barrier, we expect the localized states to show stronger shift than the delocalized ones, and we also expect the above the barrier Bragg states E_B and HH_B to show stronger shifts than the bound states E_1 and HH_1 and E_2 and HH_2 due to a larger ''effective QW size'' that is now the size of the ACQW.

The estimation of the induced electric dipole in an ACQW has been treated both by calculating the nonlinear optical rectification[12] and by solving the rate equations for the coupled three levels E_1, E_2, and E_3 via the optical field.[9] The induced field by both methods was found to be proportional to the flux of the infrared photons. Hence, to evaluate the shifts induced by the local electric field F_{local} we define F_{local} by

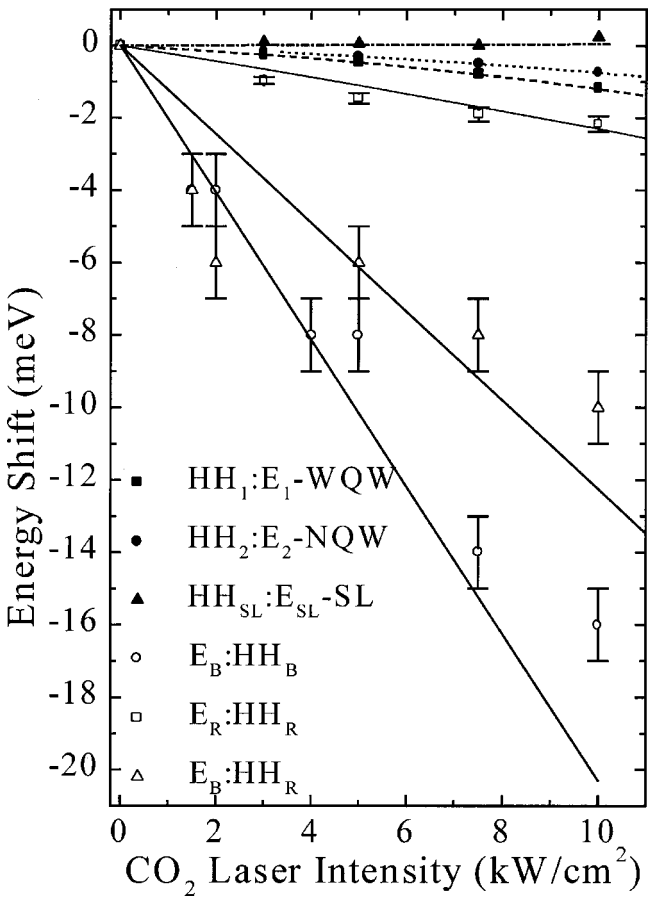

FIG. 9. Energy shifts of the bound and continuum energy levels under various infrared excitation intensities: solid squares- $E_1{:}HH_1$, solid circles- $E_2{:}HH_2$, solid triangles- $E_{\mathrm{SL}}{:}HH_{\mathrm{SL}}$, open squares- $E_R{:}HH_R$, open circles- $E_B{:}HH_B$, open triangles- $E_B{:}HH_R$.

$$F_{\mathrm{local}} = \alpha\Phi \tag{4.4}$$

where Φ is the infrared photon flux and α is a constant to be fitted to the data with the constraint that this parameter must be the same for all the energy levels. This way we can estimate the induced local field in Fig. 9 we summarize the effect of the modulating field on all the different energy levels, bound and above the barrier states.

1. Levels bound inside the well

Figure 9 shows the redshift of the three bound transitions $E_1{:}HH_1$, $E_2{:}HH_2$, and $E_{\mathrm{SL}}{:}HH_{\mathrm{SL}}$ as a function of the infrared excitation intensity. When the IR excitation power intensity increases, i.e., when the generated dc electric field increases, the redshifts of these energy transitions increase in accordance with Eq. (4.2). Furthermore, the magnitude of the shifts depends on the QW size, the WQW shows a larger shift than the NQW as predicted by Eq. (4.2). On the other hand, the transition $E_{\mathrm{SL}}{:}HH_{\mathrm{SL}}$, where the two levels E_{SL} and HH_{SL} are outside the ACQW region, does not show any shift when the localized electric field is applied as expected in the absence of heating.

The calculation of the energy shifts using Eq. (4.2) is plotted by dashed lines in Fig. 9 for the three bound energy levels. We considered the electrons and heavy hole wave functions of each transition and we used $\alpha = 3.5\,\mathrm{cm}\times\mathrm{sec/Coulomb}$ to calculate all the energy shifts. When the local field is generated, electrons in the WQW and NQW accumulate in the left side of the wells, while the holes accumulate in the right side of the wells, therefore they produce an electric dipole that redshifts the energy levels of these bound states. As discussed earlier, this electric dipole $D = e(\langle z\rangle_h^{n,n} - \langle z\rangle_e^{n,n})$ depends on the QW well size [Eq. (4.2)] and therefore the energy levels are shifted by an amount that is proportional to the well width.

2. Levels in the continuum

As discussed previously, three above the barrier transitions are resolved: $E_B{:}HH_B$ at 2.052 eV, $E_R{:}HH_R$ at 2.07 eV, and $E_B{:}HH_R$ at 2.082 eV. The redshifts of these levels under the infrared excitation are also reported in Fig. 9. Several results should be explained: (i) All above the barrier energy levels show stronger shifts than the bound states when subjected to the same photoinduced electric field. (ii) The transitions $E_B{:}HH_B$ and $E_B{:}HH_R$ show a strong shift when the photoinduced electric field is applied, while the transition $E_R{:}HH_R$ shows a much smaller shift. These features are related to the degree of localization and can be explained using the Stark effect model. Energy levels above the barrier that are confined in the ACQW region, can produce a much larger electric dipole than the bound states, because the charge separation between electrons and holes that is of the order of the ACQW size (270 Å) is larger than the WQW, which is the maximum charge separation of the bound states. For example, the calculated average separation between electron and heavy holes of the Bragg-confined level is $(\langle z\rangle_h^{B,B} - \langle z\rangle_e^{B,B}) \approx 60$ Å compared to a 5–6 Å for the transition $E_1{:}HH_1$ (WQW bound level) and even less for $E_2{:}HH_2$ (NQW bound level). This order of magnitude difference between the dipole moments of the bound states and the Bragg-confined continuum state, leads to the stronger shift of the Bragg-confined level as seen in Fig. 9. Using Eq. (4.2), we calculated the shifts of these continuum levels. For this calculation, we used their respective envelope wave functions and the value $\alpha = 3.5\,\mathrm{cm}\times\mathrm{sec/Coulomb}$ determined from the fit to the bound levels energy shifts. The calculated results are shown as full lines in Fig. 9 and are in good agreement with the experimental data. The same argument as the one used before explains the smaller shifts of the continuum transitions $E_B{:}HH_R$, which has a smaller dipole moment of $(\langle z\rangle_h^{R,R} - \langle z\rangle_e^{B,B}) \approx 30$ Å. These two transitions $E_B{:}HH_B$ and $E_B{:}HH_R$ form a class of highly localized transitions in the ACQW region that are strongly influenced by the photoinduced electric field localized in the ACQW.

At high excitation powers (>6 kW/cm^2) there are deviations of the experimental data of the two highly localized

levels $E_B{:}HH_B$ and $E_B{:}HH_R$ (Fig. 9, open triangle and open squares) from the calculated lines. The experimental values are smaller than predicted by our model. These deviations of the experimental data at high excitations of the CO_2 laser stem from the saturation of the Stark effect. At high photoinduced electric fields, the carriers tend to accumulate in the opposite sides of the ACQW, this accumulation results in a saturation of the dipole moments of the two localized levels $(\langle z\rangle_h^{B,B}-\langle z\rangle_e^{B,B})$ and $(\langle z\rangle_h^{R,R}-\langle z\rangle_e^{B,B})$ which leads to a smaller increase of the energy shifts.

On the other hand, the transition $E_R{:}HH_R$ has a much smaller shift under infrared excitation than the other two transitions $E_B{:}HH_B$ and $E_B{:}HH_R$. The electrons and holes of this above the barrier transition are mostly localized in the reflector region, hence, the joint density of electrons and holes in the ACQW region is much smaller than that of $E_B{:}HH_B$ or $E_B{:}HH_R$, resulting in a much smaller influence of the electric dipole. As a result, this state is less affected by the localized field and, therefore, shows smaller shifts. This confirms that this state belongs to a different class of continuum states that are mainly confined in the reflector region rather than in the ACQW region.

V. CONCLUSIONS

In conclusion, by inserting Bragg reflectors on each side of an asymmetric coupled quantum well, by applying a photoinduced local electric field, and by using MRRS and MPL probes, we identify two kinds of localized states at energies above the barrier. The first kind includes the transitions $E_B{:}HH_B$ and $E_B{:}HH_R$, which are localized in the ACQW region. As seen by MRRS measurements, these levels show a relatively large redshift when modulated by a local static photoinduced electric field in the ACQW region. The second kind of transition $E_R{:}HH_R$, extends mainly in the reflector region and as a result, it shows a much smaller shift under the influence of the same electric field. The generation of the local field in the ACQW modifies the energy levels spectrum of bound and above the barrier levels, using the Stark shift model we explained quantitatively the energy shifts of these levels.

ACKNOWLEDGMENT

This research was supported by the Israel Science Foundation founded by the Israel Academy of Sciences and Humanities.

[1] J. E. Zucker, A. Pinczuk, D. S. Chemla, and W. Wiegmann, Phys. Rev. B **29**, 7065 (1984).
[2] G. Lenz and J. Salzman, Appl. Phys. Lett. **56**, 871 (1990).
[3] F. Capasso, C. Sirtori, J. Faist, D. L. Sivco, S. G. Chu, and A. Y. Cho, Nature (London) **358**, 565 (1992).
[4] C. Sirtori, F. Capasso, J. Faist, D. L. Sivco, S. G. Chu, and A. Y. Cho, Appl. Phys. Lett. **61**, 898 (1992).
[5] B. Sung, H. C. Chui, E. L. Martinet, and J. S. Harris, Jr., Appl. Phys. Lett. **68**, 2720 (1996).
[6] M. Zahler, I. Brener, G. Lenz, J. Saltzman, E. Cohen, and L. Pfeiffer, Appl. Phys. Lett. **61**, 949 (1992).
[7] M. Zahler, E. Cohen, J. Saltzman, E. Linder, E. Maayan, and L. Pfeiffer, Phys. Rev. B **50**, 5305 (1994).
[8] M. Zahler, E. Cohen, J. Saltzman, E. Linder, and L. Pfeiffer, Phys. Rev. Lett. **71**, 420 (1993).
[9] M. Bendayan, R. Kapon, R. Beserman, A. Sa'ar, and R. Planel, Phys. Rev. B **56**, 9239 (1997).
[10] F. Stern and S. Das Sarma, Phys. Rev. B **30**, 840 (1984).
[11] G. Bastard, *Wave Mechanics Applied to Semiconductor Heterostructures* (Halsted, 1992).
[12] E. Rosencher, Ph. Bois, B. Vinter, and D. Kaplan, Appl. Phys. Lett. **56**, 1822 (1990).
[13] J. Wang, J. P. Leburton, and J. E. Zucker, IEEE J. Quantum Electron. **30**, 989 (1994).
[14] T. Worren, K. B. Ozanyan, O. Hunderi, and F. Martelli, Phys. Rev. B **58**, 3977 (1998).